I R A M P
7(2), Dec. 2016, pp. 91-101

ISSN: 2229-3159

Laser-induced Plasma Spectroscopy of Singly Ionized Nitrogen lines for Determination of Transient Plasma Parameters

ASHRAF M. EL SHERBINI,[1] AHMED T. HASSAN,[2] AND CHRISTIAN G. PARIGGER[3*]

[1]Laboratory of Laser and New Materials, Faculty of Science, Cairo University, Egypt
[2]Department of Physics, College of Science, Al Imam Muhammad Ibn Saud Islamic University, Al Riyadh, KSA
[3]The University of Tennessee / University of Tennessee Space Institute, Center for Laser Applications, 411 B.H. Goethert Parkway, Tullahoma, TN 37388-9700, USA
[*]Corresponding author E-mail: cparigge@tennessee.edu (C.G. Parigger)

ABSTRACT: Electron density and temperature were measured with a temporal resolution of 10 ns subsequent to laser-induced optical breakdown in standard ambient air. The micro-plasma was generated near a flat aluminum target using IR Nd: YAG laser radiation and recorded using an echelle spectrograph equipped with an intensified charge coupled device. Two complimentary methods were employed in the analysis. First, a Boltzmann plot was constructed to infer temperature from the relative spectral intensity of recorded N II ionic lines that appeared for a time delay of 20 ns at the wavelengths of 463.05, 517.9, 500.33, and 567.9 nm. The electron densities were simultaneously measured utilizing the Stark broadened singly ionized nitrogen lines at 500.33 nm and 567.9 nm. And second, the absolutely calibrated spectral radiance and emission coefficient of the plasma continuum were utilized to independently determine the plasma parameters. The average temperatures were found to decrease from 13.5 eV to 2.4 eV for time delays of 0 ns to 150 ns, respectively. The measured, corresponding electron densities diminished from 7.4×10^{19} cm^{-3} to 0.8×10^{19} cm^{-3}. Both methods yielded consistent results, thereby confirming the use of absolutely calibrated data in analysis of transient air micro-plasma within the first 150 ns.

PACS Codes: 52.38.Mf, 52.70.-m, 32.30.-r, 52.25.Jm, 42.62.Fi, 82.80.-d

Keywords: Laser ablation, plasma diagnostics, atomic spectroscopy, plasma spectroscopy, laser-induced breakdown spectroscopy, nitrogen.

1. INTRODUCTION

Laser induced plasma spectroscopy (LIPS) is devoted to the physics of plasma excited by the interaction of pulsed, high peak-power laser radiation with targets that in general include solids, liquids and gases. Passive optical emission spectroscopy technique (OES) is used to explore these plasmas by measuring the spectral distribution with respect to wavelength of the emitted light. The determination of electron density and excitation temperature is an essential aspect of plasma diagnostics [1 - 6]. The measurements are based on a well-established physics to include specifically electromagnetic theory, classical thermodynamics, statistical physics, and quantum mechanics of atoms and molecules in what is called LIPS that standing for laser induced plasma spectroscopy. Concurrently, laser-induced breakdown spectroscopy (LIBS) has gained much attention during the last four decades to describe a technique or protocol followed frequently by analytical chemists and engineers in different applied fields. The primary aims in LIBS include, first, the identification of different elements in a solid target matrix from recorded spectral line or spectroscopic "fingerprints", and second, the measurement of relative concentrations of the ingredients of the target [7 - 10]. However, LIBS continues to show challenges, for example, the improvement of the current state-of-the-art limit of detection (LOD) [8 - 11], or the occurrences of spectral line shifts and mostly interferences between lines from different elements in matrix alloys that may cause difficulties in analysis of the measured spectra. However,

the majority if not all authors elaborate on spectroscopy of emitted radiation following laser-induced optical breakdown for relatively long time delays.

The radiation emitted from the laser spark is found to depend on the plasma thermodynamical state [1 - 6]. For relatively large electron densities, n_e, of the order of 10^{19} cm^{-3} (0.37 amg), the plasma frequency [12], $\nu_p = 12\pi\left(n_e e^2/\varepsilon_0 m_e\right)^{1/2}$, amounts to $\nu_p \approx 8{,}900\times\sqrt{n_e(cm^{-3})} \approx 2.8\times10^{13}$ Hz, the electron collision frequency [12], $\nu_c = 2.92\times10^{6} n_e(cm^{-3}) \ln\Lambda\left(T_e(eV)\right)^{-3/2}$, equals $\nu_c = 1.1\times10^{13}$ Hz for the Coulomb logarithm [12], $\ln\Lambda = 3.5$, and an electron temperature, T_e = 50,000 K (4.4 eV), and is large enough for equilibration of the different plasmas species: Atoms, ions, electrons and radiation. The plasma emits continuum radiation like a black or gray body, *i.e.*, the continuous radiation field spreads over the UV, visible and IR wavelength ranges. The continuum originates essentially from two channels, namely from free-bound transitions in which fast plasma electrons recombine with some ion continuum states leading to radiative recombination with spectral broadband and individual line spectra, and/or free-free transition which occur due to deceleration of fast electrons in the electromagnetic fields of the atoms and ions in plasma leading to bremsstrahlung radiation [1 - 6]. For a relatively large temperature of the order of 116,000 K (10 eV) the longer wavelength side of the continuum spectral features are dominated by the free-free transition with inverse square wavelength dependence [6], and the shorter wavelength side contributions are attributed to free-bound recombination radiation that strongly depends on temperature [6].

As time elapses, in the microsec delays, i.e. the range at which the LIBS- technique is ofttен applied, the plasma loses its internal energy due to isentropic expansion [13 - 16] and radiative deceleration and/or recombination, and hence, the concentration of the free electrons diminishes to values of the order of 10^{17} cm^{-3}. The plasma frequency decreases to $\approx 2.8\times10^{12}$ Hz, the electron collision frequency reduces to $\nu_c = 1.2\times10^{10}$ Hz for $\ln\Lambda = 3.9$ and T_e = 11,600 K (1 eV) but equilibrium between particle species can be sustained. The plasma state is usually considered to be in local thermodynamical equilibrium (LTE) [17 - 19] and one encounters and measures line spectra as superimposed componant on the continuum contributions [1 - 10]. The LTE condition would be determined via relation [17 - 19] which is usually satisfied,

$$n_e >> 1.6\times10^{12}\sqrt{T_e}(\Delta E)^3 cm^{-3}, \quad (1)$$

for energy differences, ΔE, of the order of 5 eV and for a temperature, T_e, of 10,000 K, the LTE condition for LIBS leads to $n_e^{LIBS} >> 0.2\times10^{17}$ cm^{-3}. The local thermodynamic equilibrium condition is frequently encountered in analysis with LIBS - usually experiments are designed for measurement of spectral signatures for time delays that range from 1 to 10 μs after optical breakdown. For such time delays, the plasma emission lines with energy differences are stable enough to maintain an elemental "fingerprint," moreover, the emission lines show minute or inconsequential spectral line shifts. In this work, the electron densities are 1.1 up to 7.5 × 10^{19} cm^{-3}, with energy differences of typically 20 eV, electron temperatures of 0.8 to 13.5 eV, respectively. The LTE condition is certainly met, $n_e >> 0.5$ to 0.3 × 10^{19} cm^{-3} and the expansion dynamics may cause redistribution of the electron density [20] in the early plasma decay yet the measurements are designed to record line-of-sight averaged data in this work.

A number of articles are available in the literature addressing phenomena at the microsecond time scale associated with LIBS [21 - 24], and plasma diagnostics yields temperatures in the range of 8,000 - 25,000 K (0.7 - 2 eV) and average densities in the range of 1 to 7 × 10^{17} cm^{-3}. The plasma parameters are to be interpreted with the existence LTE, viz., the plasma is cool enough due to loss of its internal energy in the adiabatic expansion process against ambient air at standard ambient temperature and pressure (SATP). However, compared to the large number of publications at the microsecond time scale, a relatively small number of works investigates plasma characteristics at the nanosecond time scales [14, 25 - 26].

Temperatures of the order of 116,000 K (10 eV) during the first tenths of nanoseconds decrease to 25,000 K (2 eV) for time delays of hundreds of nanoseconds along with a change of the electron densities [14] from typically $5 - 0.8 \times 10^{19}$ cm^{-3}. Recently communicated measurements [14] were analyzed using the absolute emission coefficient in (Watt/ m^3 nm sr) of the continuum component in the near IR wavelength region.

In this work, we have adpted LIPS, the results are presented for values of plasma parameters using optical emission spectroscopy (OES) for time delays from 0 to 150 ns with fixed narrow gate-open duration of 10 ns. Boltzmann plots were constructed to determine the electron temperatures utilizing the N II ionic lines at 517.9, 500.33, 567.9 and 463.05 nm. The Stark broadened N II ionic lines at 500.33, 567.9 nm were employed to measure electron density. These measurements are compared to predictions of the absolute calibration measurement, and in turn, the comparisons can verify the absolute calibrations.

2. EXPERIMENTAL METHODS

The experimental setup is effectively identical to that used previously [2]. It comprises a Nd:YAG laser device that can deliver an energy of 450 mJ per pulse of 5 ns duration at the fundamental wavelength of 1064 nm. The laser light was brought to the focus using a multi-layer coated plano-convex lens of focal length 10 cm. An aluminum flat target with small traces of magnesium was positioned at a distance of 9 cm in front of the lens that was used for focusing the laser radiation, consequently, optical breakdown occurred only at the sample.

The emitted light from the plasma was collected at the entrance of a SE 200 echelle type spectrograph via a 25 µm optical fiber. In the experiment reported here, a glass fiber was used to avoid 200 nm to 400 nm contributions in the 400 nm to 800 nm wavelength region of interest. The fiber was positioned at a distance of 5 ± 0.1 mm transverse to the laser-plasma expansion axis using an xyz holder that was designed to achieve a resolution of 100 ìm. The spectrograph has resolving power of 2500. The rectangular shaped exit port of the spectrograph is connected to an ultra-fast ICCD-camera type Andor-iStar model DH734-18F, with a minimum rise time of 25 ps and a pixel size of 196 $ìm^2$.

Signals from the entire laser ablation plume are recorded. Data acquisition is controlled via a computer interface and the supplied KestrelSpec94 software that allows one to adjust time delay and gate-open duration as well as the gain level of the camera. Moreover, the software includes a background subtraction option, particularly useful for correction of stray light noises. The laser energy was monitored using previously calibrated glass beam plates [3] that absorb 4% and reflect 5%.

The laser spot size was determined at the target potion using calibrated, thermal sensitive paper available from the Quantel Laser company. The circular shape reveals a diameter of 0.5 ± 0.1 mm. The irradiance level of 12 ± 1 GW/cm^2 was kept constant during the experiments. The spectrograph wavelength scale was calibrated using a low pressure Hg-lamp (model Ocean optics HG1), while the spectral intensity (vertical axis) was calibrated in absolute units of Watts using DH standard deuterium-halogen light source (model Ocean Optics DH-2000-CAL) [4]. For improvement of the signal-to-background ratio, the recorded spectra data points are collected over 50 consecutive laser shots on a rotating target. In order to address the emission from the ambient air breakdown in laser focus, the target was removed to find that air breakdown plasma was initiated 9.7 mm from the focusing lens. Subsequently, the target was positioned at a slightly closer distance from the same lens, *i.e.*, at 9 cm.

The trigger jitter of camera with respect to the provided Q-switch trigger was measured to be peak-peak 3 ns, or amplitude RMS of 1 ns. An ultra-fast, 10 ps rise-time photo diode was employed to record the time delay of the laser pulse and of camera gate open during the experiment. This was accomplished by using a beam splitter to reflect 4 % of the laser beam and by displaying both diode- and gate-open- signals on an oscilloscope. Zero time delay coincides with cessation of the laser pulse. This was determined by adding 5 ns to the laser- and gate-open- time delay at which optical breakdown light emission commences.

3. RESULTS AND DISCUSSION

In the experiment, a flat aluminum target was irradiated by 450 mJ, 6 ns Nd:YAG pulses at the wavelength of 1046 nm. The spot size of diameter 0.5 ± 0.1 mm ensures a constant irradiance level of 12 ± 1 GW/cm^2. This level of irradiance is well above threshold for plasma generation [7]. A gate time of 10 ns was used and the delay was changed in equal steps of 10 ns up to 150 ns. At the early time delays, the plasma rapidly expands and emits like a gray body [6], *i.e.*, the continuum component dominates the emission spectra, especially at the first few tenth of nanoseconds. The plasma can be described as being close to complete thermodynamical equilibrium (CTE). Line-of-sight measurements yield averages of electron density, n_e, and excitation temperature, T_e, in support of CTE. Yet the early expansion dynamics include occurrence of laser-supported detonation waves that usually show gradients of n_e and T_e across the shock waves or stagnation areas for colliding shock waves. The averages of electron density and temperature distributions are consistent with isentropic expansion. As the time delay increases, the continuum contributions decrease and spectral lines originating from the N II ionic lines at the wavelengths of 463.04, 500.33, 517.9 and 567.9 nm increase relative to the continuum. This may indicate that the plasma state is approaching the local thermodynamical equilibrium (LTE) [17 - 19].

In the emission spectra, other broad N II lines slightly above the continuum can be identified. The hydrogen H_α line and neutral oxygen are not yet noticeable due to the relatively large electron number density and small hydrogen oncentrations in SATP air for the early time delays, but these lines are usually measured as the plasma cools. Two N II lines 648.2 nm and 660nm near the hydrogen H_α line are not well-developed during the first 100 ns following optical breakdown [27] but it starts to appear as delay of 150 ns. Other N II ions like 444.7 nm and 399.5 nm with excitation energy of 23.2 and 21.9 eV are not further elaborated because the 500.33 nm line is sufficient for the determination of electrons density.

Figure 1 illustrates the emission spectra from the plasma after carrying out the procedures of absolute calibration with details presented previously [14]. The strong continuum component that appears at the longer wavelength region indicates hot plasma. The fitting of the continua was carried out using the Planck function. Temperature was used as the fitting parameter. The following electron excitation temperatures were inferred: 156, 78 and 54 kK (13.5, 6.8 and 4.7 eV) for 0, 50 and 90 ns time delays, respectively. The measured temperatures appear to be larger

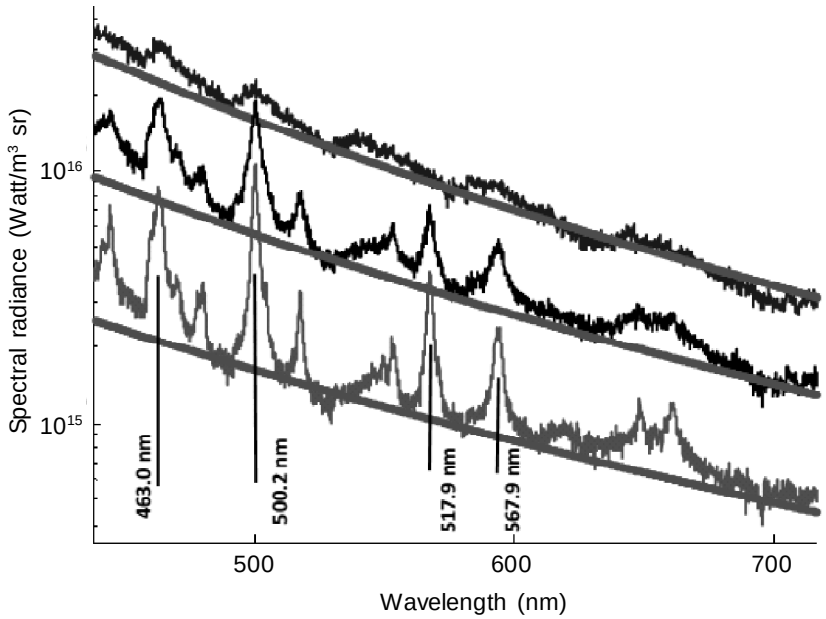

Figure 1: Absolutely calibrated plasma emission spectra and fitted Planck functions (red) indicate electron temperatures of 145, 78 and 27 kK from top to bottom for time delays of 10 ns (online color blue), 50 ns (online black) and for clear demonasrtration at 150 ns (online color green). Pronounced spectral N II lines are precisely identified and labeled

than usually reported in different LIBS experiments conducted in SATP air. However, the applied absolute calibration procedures [14] are based on well-known plasma spectroscopy [7].

Temperature values obtained from the absolute calibration method were compared with results from relative intensities of the N II ionic lines by constructing Boltzmann plots. Table 1 summarizes the atomic constants that were utilized.

Table 1
Atomic parameters of N II ionic lines used for analysis with Boltzmann plots

λ (nm)	*Transition probability (s^{-1})*	*Statistical weight*	*Energy (eV)*	*Stark broadening (nm)*
463.05	7.72×10^7	5	21.16	–
500.33	1.10×10^8	8	23.12	0.025 ± 50%
517.9	1.07×10^8	9	30.13	–
567.9	4.96×10^7	7	20.66	0.021 ± 55%

Figure 2 (a) and (b) display the Boltzmann plots for time delays of 20 and 50 ns. The Boltzmann plots indicate fitted straight lines of negative slope. The measured line intensities appear to be perfectly aligned with the fit, therefore, one can infer absence of self-absorption. Relatively large temperatures are predicted: 11.2 and 6.8 eV at time delays of 20 and 50 ns, respectively.

Figure 3 displays the line-of-sight temperature variation with time delay. The Boltzmann plot method is applied

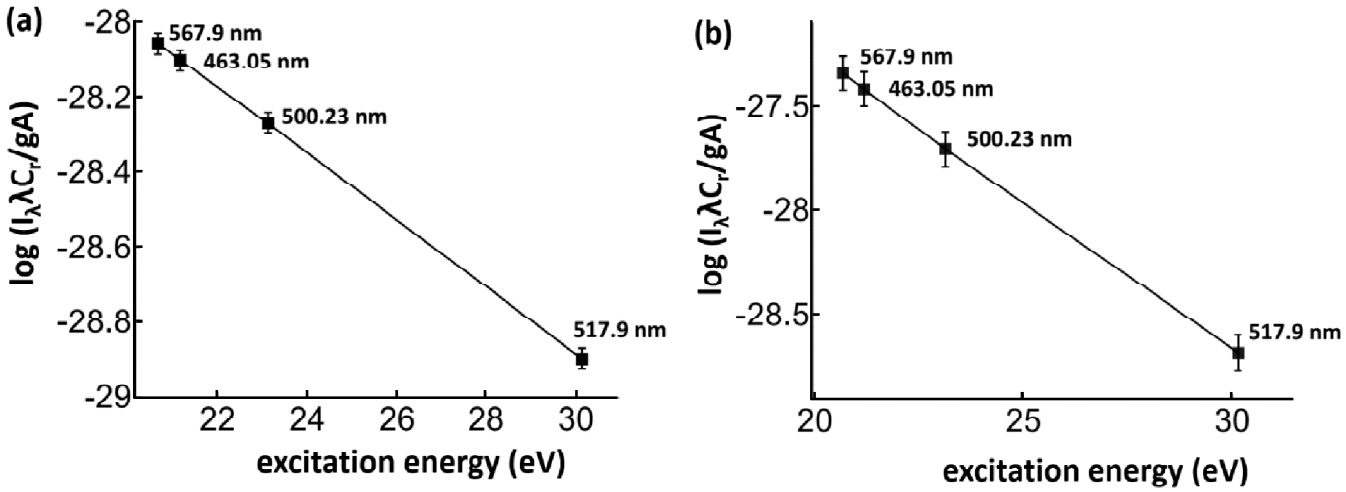

Figure 2: Boltzmann plots using N II lines as shown at (a) 20 ns and (b) 50 ns time delay. The predicted temperatures amount to 11.2 ± 0.3 and 6.8 ± 0.5 eV, respectively

for each of the 9 data sets obtained within the first 100 ns after optical breakdown.

A verification of the temperatures determined with Boltzmann plots can be accomplished utilizing absolute calibration procedures [14]. Table 2 summarizes the results. Excellent agreements are obtained for the temperatures measured by use of largely different methods. In turn, the results verify the correctness of the calibration procedures for absolute calibration.

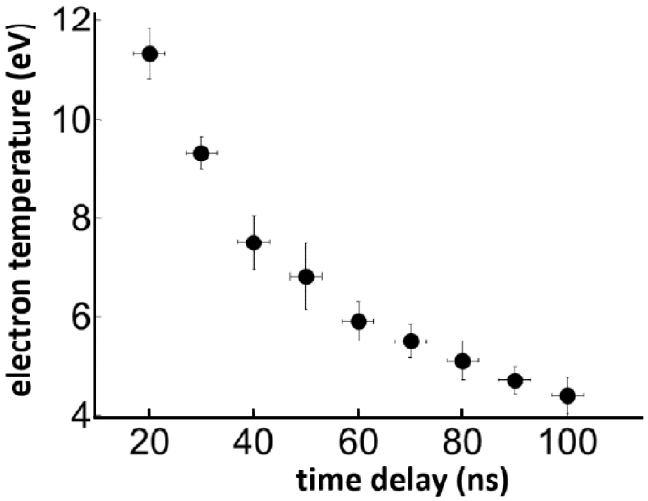

Figure 3: Electron temperature (1 eV = 11,600 Kelvin) variation with time delay from optical breakdown, deduced from N II ionic lines using Boltzmann plots. Horizontal error bars correspond to the selected gate-open durations used in the experiments. The vertical error bars reflect the errors in the integrated line intensities and the uncertainties in the atomic parameters listed in Table 1

Table 2
Measured electron temperature, T_e, and density, n_e, for different time delays, τ_d, and fixed 10 ns gate width, inferred from Boltzmann plot and Stark-broadened N II lines and separately from absolute calibration and Planck function fitting. The electron densities n_e^1 and n_e^2 are measured from the N II lines at 500.33 nm and 567.9 nm, respectively. Absolute calibration results are indicated with the superscript A

τ_d (ns)	$T_e^B(eV)$	$n_e^1(10^{19}/cm^{-3})$	$n_e^2(10^{19}/cm^{-3})$	$T_e^A(eV)$	$n_e^A(10^{19}/cm^{-3})$
0	-	-	-	13.5	7.3
10	-	-	-	12.5	6.1
20	11.2	4.8	4.8	11.5	4.8
30	9.3	3.5	3.3	9.5	3.5
40	7.5	2.5	2.5	7.8	2.5
50	6.8	2.23	2.1	6.8	2.3
60	5.9	1.7	1.9	5.9	1.8
70	5.5	1.5	1.7	5.5	1.6
80	5.1	1.3	1.35	5.0	1.35
90	4.7	1.18	1.2	4.7	1.1
100	4.4	1.1	1.1	4.3	1.0
150	2.4	0.90	0.87	2.5	0.86

The electron number density was measured from Stark broadening of N II ionic spectral lines [31] and from the measurement of the absolute emission coefficient of the continuum component in the units of (Watt/ m^3 nm sr) at the longer wavelength region [14]. For the former method, results of Stark broadening calculations for the well-studied N II ionic line at 500.33 nm are utilized [31].

Furthermore, the N II ion line at the wavelength of 567.9 nm can also be utilized to determine the electron density. Figure 4 illustrates recorded spectra for different time delays.

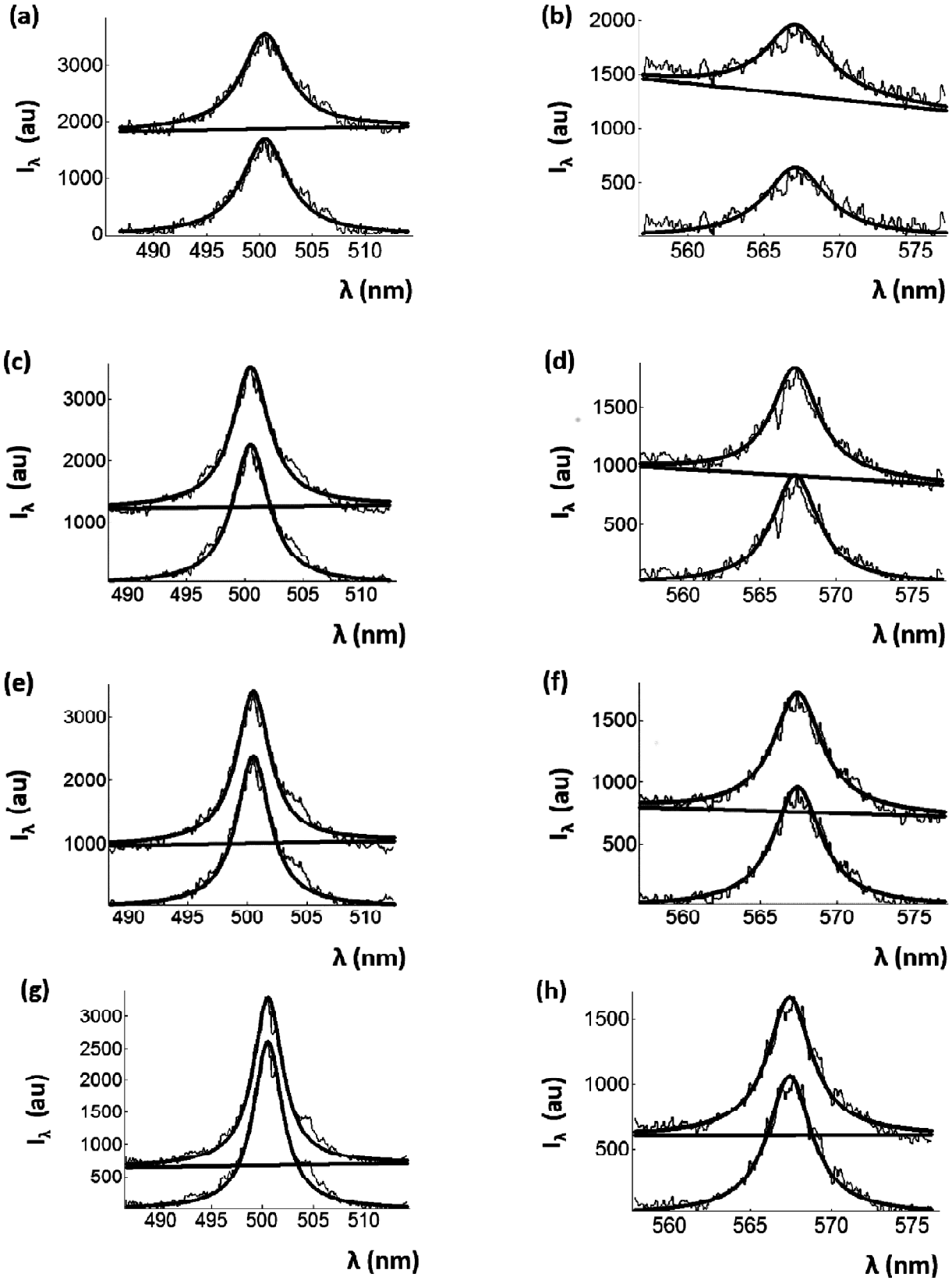

Figure 4: Comparisons of Voigt fitting relative intensity, I_λ, versus wavelength, λ, to the spectral N II lines at 500.33 nm (left) and 567.9 nm (right) for (a) and (b) 30 ns, (c) and (d) 50 ns, (e) and (f) 70 ns and (g) and (h) 100 ns time delays

For the ionic N II lines, the electron densities, n_e, are determined using;

$$n_e(cm^{-3}) \approx \Delta\lambda_S(nm)\left(\frac{N_r(cm^{-3})}{\omega_S(nm)}\right) \tag{2}$$

The Stark broadening parameters for both lines are summarized in Table 1. Voigt fitting is applied to find the full-width-at-half-maximum of the Lorentzian component, $\Delta\lambda_S$, of the two N II lines. The Stark broadening parameter, ω_S, indicates the width at reference electron density [2], $N_r = 10^{17}$ cm^{-3}.

In Equation (2), Doppler contributions are omitted but these would indicate a broadening of 0.3 nm for the range of electron densities and temperatures of interest in this work. Van der Waals and resonance broadening are also omitted since molecular collisions are absent, and the transitions taken into consideration are not of resonant nature, see Table 1. The ionic effects are found to be very small and hence can be neglected as well - no line asymmetry was observed for the 500.33 and 567.9 nm lines. In Figure 4, strong continuum components appear as indicated by the almost straight lines (online color green) especially for the early time delays. The magnitude and slope of the background diminishes, thereby indicating a decrease in the electron density values. The results of the measurement of electron density using either line were found nearly identical. The results in columns 3 and 4 of Table 2 agree nicely with the results obtained applying absolute calibration procedures, discussed below.

For the latter method, the electron density,

$$n_e^A(cm^{-3}) \approx 9\times10^{13}\,\lambda(nm)\left(\varepsilon_\lambda^{ff}\sqrt{\frac{T_e(eV)}{13.6}}\right)^{1/2}, \tag{3}$$

can be determined from the absolute emission coefficient, ε_λ^{ff} (W/(m^3 nm sr)), at near IR wavelengths of 750 nm, and from the estimated electron temperature, T_e (eV), ratio with respect to the 13.6 eV ionization energy of hydrogen. The results of the absolute calibration measurements are included in the last two columns of Table 2. The electron temperature range is from 13.5 to 4.3 eV, and the electron density is as high as (7.3 ± 0.8) × 10^{19} cm^{-3} for 0 time delay, monotonically decreasing to (1.1 ± 0.3) × 10^{19} cm^{-3} at 100 ns time delay.

Figure 5 displays the variation of the measured density versus time delay as inferred from the 500.33 nm N II line. The results for the electron densities are expected to agree for both N II lines at 500.33 and 567.9 nm. Fig. 6 confirms that the results indeed agree: The slope amounts to ~ 1 within error bars.

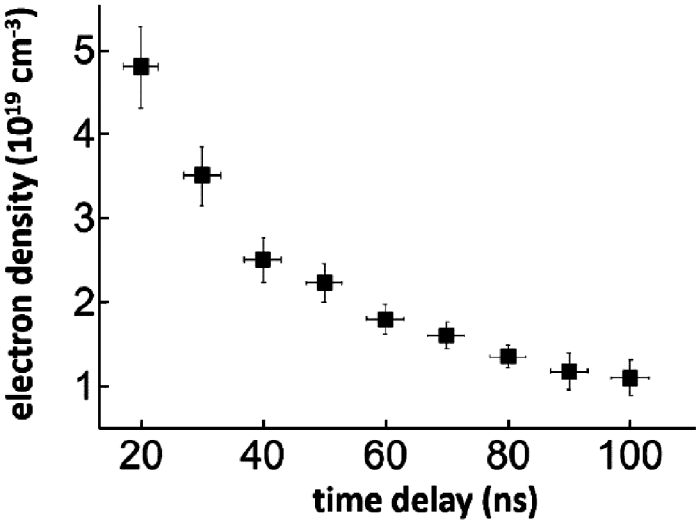

Figure 5: Variation of electron density as calculated utilizing the 500.33 nm N II line with time delay

The agreement indicated in Figure 6 further reveals that the 567.9 nm N II line is reliable for the measurement of the electron density during the early time delays especially when the $H_{\acute{a}}$ is broad and not discernible from the continuum. The reported measurements appear consistent with previously communicated aspects of the measurement of electron density [27, 29].

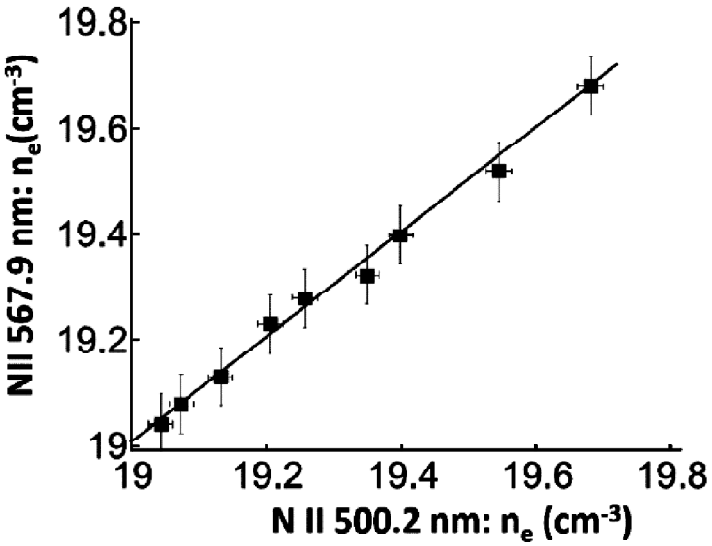

Figure 6: Electron density from 500.33 nm N II line (abscissa) and density using N II line at 567.9 nm (ordinate) with a slope of 0.98 ± 0.2

During the early time delays, the plasma expansion process is almost adiabatic or isentropic [14 - 15, 30]. For the relative specific heat factor of $\gamma = C_p/C_V$, classical thermodynamics allows one to determine the relation between density and temperature of plasma during adiabatic expansion,

$$\frac{T_e}{n_e^{0.67}} = \text{constant.} \tag{4}$$

Figures 7 (a) and (b) elucidate the density and temperature correlation in graphical form. Fig. 7 (a) shows the results from measuring the plasma parameters from absolute calibration indicating a slope of 0.63 ± 0.24. Fig. 6 (b)

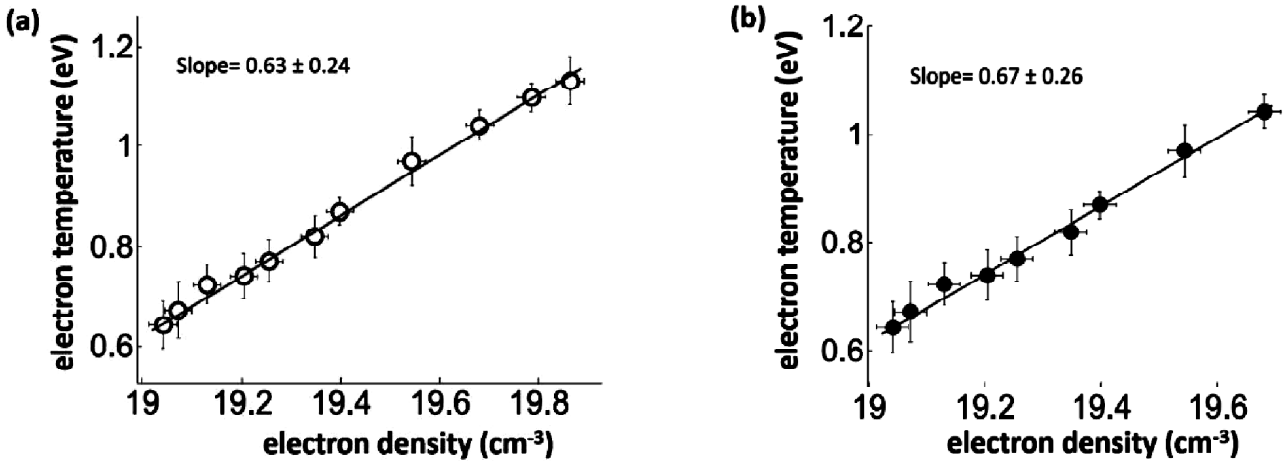

Figure 7: Log-log plot of the temperature density relation from (a) absolute calibration and (b) from the N II line at 500.33 nm

indicates a slope of 0.67 ± 0.26, measured with classical optical emission spectroscopy, namely, Stark broadening of the N II line at 500.33 nm and temperature from Boltzmann plots.

Both results agree nicely within the error margins, confirming the invariance of the quantity $T_e / n_e^{0.67}$ for the average electron temperature and density of isentropic plasma expansion for early time delays from optical breakdown.

It is worth noting that the recorded spectra in this article can be attributed to the emissions from the created dense layer of nitrogen gas surrounding the target material during fast plasma expansion in the first few tenth of ns regimes [14]. This thin external layer of nitrogen plasma is activated to emitt a strong nitogen ionic lines via two chanelles; the emitted fast electron coliisional ionization and the photo ionization by the intense UV component emitted from the plasma core [30, 32]. This layer could be useful for several applications that need to hot and intense sources of UV emissions.

4. CONCLUSIONS

In conclusion, electron density and temperature that describe laser-induced plasma in ambient laboratory air are expected to be of the order of 0.8 to 7 × 10^{19} cm^{-3} and 2.5 to 13 eV, respectively, for early time delays from optical breakdown. These results are determined using classical emission spectroscopy to find electron density and temperature from Stark widths and Boltzmann plots, and by using absolutely calibrated spectra. The N II line at 567.9 nm was identified as a reliable measure of electron density in the early delay times of several tenth of ns. The results for temperature are about one order of magnitude larger than usually communicated in the description of experiments using LIBS in the microsec delay range. The expansion phenomena are found to be adiabatic in nature. A thin, hot and dense layer is created that shows variation of the electron density across the expanding plasma. These details appear only tangentially of interest in LIBS practice, although current works in the literature indicate that several groups discuss applications of plasma confinement or plasma stagnation phenomena associated with expanding electron density waves.

Acknowledgments

The authors acknowledge the continued interest and comments from Professor Th. M. EL Sherbini and thank for support in part by the Center for Laser Applications at the University of Tennessee Space Institute and in part by the Laboratory of Laser and New Materials at Cairo University.

References

[1] H. R. Griem, *Plasma Spectroscopy*, McGraw-Hill, Inc., USA, 1964.

[2] H. R. Griem, *Spectral Line Broadening by Plasmas*, Academic Press, New York, USA, 1974.

[3] H. R. Griem, *Principles of Plasma Spectroscopy*, Cambridge University Press, UK, 1997.

[4] W. Lochte Holtgreven, *Plasma Diagnostics*, AIP Press, New York, USA, 1995.

[5] H. Hora, *Plasmas at High Temperature and Density Applications and Implications of Laser-Plasma Interaction*, Springer Verlag, Heidelberg, DE, 1991

[6] H.-J. Kunze, *Introduction to Plasma Spectroscopy*, Springer Verlag, Berlin, 2009.

[7] D. A. Cremers, L. J. Radziemski, *Handbook of Laser-Induced Breakdown Spectroscopy*, John Wiley & Sons Ltd, USA, 2006.

[8] A. Miziolek, V. Palleschi and I. Schechter, *Laser-Induced Breakdown Spectroscopy (LIBS) Fundamentals and Applications*, Cambridge University Press, UK, 2006.

[9] J.P. Singh, S. Thakur, *Laser-Induced Breakdown Spectroscopy*, Elsevier, Oxford University Press, UK, 2007.

[10] R. Noll, *Laser-Induced Breakdown Spectroscopy Fundamentals and Applications*, Springer-Verlag, Heidelberg, DE, 2012.

[11] D. Hahn, N. Omenetto, *Appl. Spectrosc.* **66** (2012) 437.

[12] J.D. Huba, *NRL Plasma Formulary*, Naval Research Laboratory, Washington, DC, 2013.

[13] H. Sobral, R. Sanginés, *Spectrochim. Acta Part B* **94-95** (2014) 1.

[14] A.M. EL Sherbini, A. M. Aboulfotouh, C.G. Parigger, *Spectrochim. Acta Part B* **125** (2016)152.

[15] C.G. Parigger, J.W.L. Lewis, D.H. Plemmons, *J. Quant. Spectrosc. Radiat. Transf.* **53** (1995)249.

[16] S. Eliezer, H. Hora, *Phys. Rep.* **172** (1989) 339.

[17] R.H. Huddlestone, S.L. Leonard, *Plasma Diagnostic Techniques*, Academic Press, New York, 1963.

[18] A. Thorne, U. Litzén, S. Johansson, *Spectrophysics, Principles and Applications*, Springer, New York, USA, 1999.

[19] G. Cristoforetti, A. De Giacomo, M. Dell'Aglio, S. Legnaioli, E. Tognoni, V. Palleschi, N. Omenetto, *Spectrochim. Acta Part B* **65** (2010) 86.

[20] C.G. Parigger, G. Gautam, D.M. Surmick, *Int. Rev. At. Mol. Phys.* **6** (2016) 43.

[21] C. Aragón, J.A. Aguilera, *Spectrochim. Acta Part B* **63** (2008) 893.

[22] E. Tognoni, G. Cristoforetti, S. Legnaioli, V. Palleschi, A. Salvetti, M. Mueller, U.Panne, I. Gornushkin, *Spectrochim. Acta Part B* **62** (2007) 1287.

[23] V. Narayanan, R.K. Thareja, *Appl. Surf. Sci.* **222** (2004) 382.

[24] J.A. Aguilera, C. Aragón, *Spectrochim. Acta Part B* **63** (2008)793.

[25] P.K. Diwakar, D.W. Hahn, *Spectrochim. Acta Part B* **63** (2008)1038.

[26] X. Liu, S. Sun, X. Wang, Z. Liu, Q. Liu, P. Ding, Z. Guo, B. Hu, *Opt. Express* **21** (213) A704.

[27] C.G. Parigger, L.D. Swafford, D.M Surmick, M.J. Witte, A.C. Woods, G. Gautam, *J. Phys.: Conf. Ser.* **548** (2014) 012043.

[28] C.G. Parigger, G. Gautam, A.C. Woods, D.M. Surmick, J.O. Hornkohl, *Trends Appl. Spectrosc.* **11** (2014) 1.

[29] C.G. Parigger, D.M. Surmick, G. Gautam, A.M. El Sherbini, *Opt. Lett.* **40** (2015) 3436.

[30] P. Mulser, D. Bauer, *High power laser matter interaction*, Springer, Heidelberg, DE, 2010.

[31] N. Konjević, A. Lesage, J.R. Fuhr, W.L. Wiese, *J. Phys. Chem. Ref. Data* **31** (2012) 819.

[32] S. S.Harilal, P. J .Skrodzki, A.Miloshevsky, B. E.Brumfield, M. C.Phillips, G.Miloshevsky, *Phys. Plasmas* **24** (2017) 063304.